AIMS Mathematics, 9(11): 31848–31867.
DOI: 10.3934/math.20241530
Received: 03 September 2024
Revised: 27 October 2024
Accepted: 04 November 2024
Published: 08 November 2024

https://www.aimspress.com/journal/Math

Research article

Physical significance and periodic solutions of the high-order good Jaulent-Miodek model in fluid dynamics

Wenzhen Xiong[1,*] **and Yaqing Liu**[2]

[1] School of Mathematics and Information Engineering, Xinyang Vocational and Technical College, Xinyang 464000, China

[2] School of Applied Science, Beijing Information Science and Technology University, Beijing 100192, China

* **Correspondence:** Email: xwz123165@xyvtc.edu.cn.

Abstract: Using Whitham modulation theory, this paper examined periodic solutions and the problem of discontinuous initial values for the higher-order good Jaulent-Miodek (JM) equation. The physical significance of the JM equations was discussed by considering the reduction of Euler's equation. Next, the zero- and one-phase periodic solutions of the JM equation, along with the associated Whitham equations, were derived. The analysis included the degeneration of the one-phase periodic solution and the genus-one Whitham equation by examining the limits of the modulus m of the Jacobi elliptic functions. Additionally, analytical and graphical representations of rarefaction wave solutions and periodic wave patterns were provided, and a solution for discontinuous initial values in the JM equation was presented. The results of this study offer a theoretical foundation for analyzing discontinuous initial values in nonlinear dispersion equations.

Keywords: the Jaulent-Miodek model; physically significant; Lax pair; Whitham-JM equation; periodic wave
Mathematics Subject Classification: 35Q31, 35Q51

1. Introduction

In nonlinear science, integrable nonlinear evolution equations have garnered significant attention due to their ability to describe various nonlinear phenomena in natural sciences. Soliton theory and integrable systems, being key areas of study, find numerous applications across diverse research fields, including plasma physics [1–3], fluid dynamics [4–7], nonlinear optics [8–11], and Bose-Einstein condensates [12, 13]. In 1976, Jaulent and Miodek [14] introduced a two-component integrable hierarchy by examining the one-dimensional Schrödinger equation with an energy-dependent potential,

leading to a series of Jaulent-Miodek equations. The first non-trivial member of JM hierarchy (JM1) is

$$\begin{aligned} \sigma^2 r_t &= \sigma q_x - \frac{3}{2} r r_x, \\ \sigma^2 q_t &= \frac{1}{4} r_{xxx} - q r_x - \frac{1}{2} q_x r, \end{aligned} \tag{1.1}$$

which can be obtained by certain transformations from the Kaup-Boussinesq system [15]. The second non-trivial member of JM hierarchy (JM2) is

$$\begin{aligned} \sigma^3 q_t &= \sigma \frac{1}{4} q_{xxx} - \sigma \frac{3}{2} q q_x - \frac{9}{8} r_x r_{xx} - \frac{3}{8} r r_{xxx} + \frac{3}{2} q r r_x + \frac{3}{8} q_x r^2, \\ \sigma^3 r_t &= \sigma \frac{1}{4} r_{xxx} - \sigma (\frac{3}{2} q_x r + \frac{3}{2} q r_x) + \frac{15}{8} r_x r^2, \end{aligned} \tag{1.2}$$

where σ is a real constant. When $\sigma = -1$, the JM models represent good JM equations, whereas when $\sigma = 1$, the JM models are considered bad. It is important to note that the good and bad JM equations cannot be transformed into each other through similarity transformations, as they exhibit distinct oscillation patterns and linear stability. Specifically, for the one-phase periodic solution discussed in Section 3, the good JM equation features two oscillating regions $[\zeta_4, \zeta_3]$ and $[\zeta_2, \zeta_1]$ leading to two periodic solutions. In contrast, the bad JM equation has a single oscillating region $[\zeta_3, \zeta_2]$ resulting in just one periodic solution with a different structure.

Periodic solutions depend on the specific parameters of the equation or the initial conditions of the system, and in some systems, the behavior of the dispersive shock wave may lead to the formation of periodic solutions. Studying these periodic solutions is crucial in nonlinear dispersion equations because it helps to understand and describe complex phenomena such as dispersion shock waves. An in-depth study of these solutions not only reveals the basic mechanism of the wave phenomenon, but also provides important information for practical applications such as fiber optic communications and fluid dynamics. The discontinuous initial value problem involves initial values made up of distinct constant states on either side of a jump discontinuity. Such solutions can feature two types of elementary waves: Rarefaction waves (RW) and dispersive shock waves (DSW). RWs represent smooth solutions to the flow equation, while DSWs are characterized by discontinuities. In the absence of modulation in the form of periodic propagation, due to the fact that the dispersion effect of the wave is also propagated at different speeds, the results in the change and sharpening of the waveform, resulting in the formation of shock waves. DSW is a wave phenomenon propagating in a nonlinear medium, which has important applications in optical fiber communication, laser technology, gas dynamics, and so on. In optical fiber communication, DSWs can be used for signal processing and enhance transmission efficiency, helping to reduce the effect of dispersion on signal quality. Whitham modulation theory, introduced by Whitham [16] in 1994 for analyzing wave motions in the Korteweg-de Vries (KdV) equation, is an effective approach for mathematically describing DSWs. It is assumed that the DSW can be asymptotically described as a slowly modulated periodic wave solution of the nonlinear dispersive equation with modulations of the amplitude, wavelength, and mean of the waves on a spatio-temporal scale that is much greater than the wavelength and period of the traveling wave. Subsequently, Kamchatnov [17] derived the generating function for the Whitham equations within the Korteweg-de Vries (AKNS) hierarchy and its various reductions, laying a theoretical foundation for analyzing the Riemann problem associated with the nonlinear Schrödinger (NLS) and modified

KdV (mKdV) equations. El et al. [18] conducted a comprehensive classification of discontinuous initial value problems in the context of defocusing NLS hydrodynamics. Kodama et al. [19] explored the Whitham equations pertaining to the defocusing complex modified KdV equation. Ivanov [20] classified the potential waveforms that evolve from initially discontinuous profiles for the generalized Chen-Lee-Liu equation and demonstrated a strong agreement between the numerical results and theoretical predictions. These important results lay an important theoretical foundation for the subsequent study of the discontinuous initial value problem of nonlinear dispersion equations [21–24].

Motivated by the above work, we consider the various solutions of the high-order good Jaulent-Miodek (JM) equation [14, 25]:

$$\begin{aligned} q_t &= -\frac{1}{4}q_{xxx} + \frac{3}{2}qq_x - \frac{9}{8}r_x r_{xx} - \frac{3}{8}rr_{xxx} + \frac{3}{2}qrr_x + \frac{3}{8}q_x r^2, \\ r_t &= -\frac{1}{4}r_{xxx} + \frac{3}{2}q_x r + \frac{3}{2}qr_x + \frac{15}{8}r_x r^2, \end{aligned} \tag{1.3}$$

which is obtained by the scale transformation $t \to -t$ from the good JM equation (1.2) with $\sigma = -1$. Equation (1.3) is relevant across various domains in physics. It finds applications in the control theory of dynamic systems, anomalous transport phenomena, image and signal processing, condensed matter physics, fluid dynamics, optics, and plasma physics, so it is very meaningful to study the physical characteristics of JM equations. The relation between JM Eq (1.3) and the Euler-Darboux equation are constructed by Matsuno [26] through the hodograph transformation combined with Riemann's method of characteristics. A kind of finite-band solution for the simplified version of Eq (1.3) was constructed by applying the JM spectral problem [27]. Some exact solutions are obtained by the traveling wave method, sech method, and generalized exponential rational function method [28–30]. As a practical application of the JM system, Wang and Xia studied its super-Hamiltonian structure using Lie super algebras and the super trace identity [31]. Recently, the approximate analytical solution of the fractional JM equation performed with the coupled fractional variational iteration transformation technique and the Adomian decomposition transformation technique [32]. Because the JM equation has definite physical meaning, strong nonlinearity, and comes with energy-dependent Schrödinger potential, it has attracted much attention. The main aim of this paper is to investigate rarefaction waves, periodic solutions, and the step-like initial value problem associated with the good JM Eq (1.3) using the traveling wave method and Whitham modulation theory. We seek to explore the relationship between modulated and unmodulated waves, as well as to analyze the mathematical principles underlying waveform structure in intermittent initial value problems.

The structure of this paper is organized as follows. Section 2 illustrates the physical derivation of the JM system, which describes a motion of a shallow water with constant density over a flat bottom. In Section 3, the rarefaction wave solution, the periodic wave solutions, and the Whitham modulation equation of the high-order JM equation are obtained, and one solution of the high-order JM equation with step-like initial data is presented based on the traveling wave technique and a similar-self solution. The conclusions of this paper are stated in the last section.

2. The physical significance of the Jaulent-Miodek system

The Jaulent-Miodek system characterizes the dynamics of inviscid shallow water flowing over a level bed while accounting for shear effects, which can be derived from Euler's equations:

$$\begin{aligned} &\frac{\partial \mathbf{V}}{\partial t} + (\mathbf{V}\cdot\nabla)\mathbf{V} = -\frac{1}{\rho}\nabla P + \mathbf{g}, \\ &\nabla\cdot\mathbf{V} = 0. \end{aligned} \tag{2.1}$$

In this context, $\mathbf{V}(x, y, z, t)$ represents the fluid velocity at the spatial coordinates (x, y, z) and time t, ρ denotes the constant density of the fluid, $P(x, y, z, t)$ is the pressure within the fluid, and $\mathbf{g} = (0, 0, -g)$ signifies the constant acceleration due to Earth's gravity [33, 34].

Set up a coordinate system, see Figure 1, where the flat bottom is positioned at $z = 0$, the flow occurs in the x-direction, and the physical variables are independent of y. Given that h represents the mean water level, $\eta(x, t)$ describes the water surface shape, and L is the typical wavelength, at the surface $z = h + \eta$, the pressure P equals P_A, so the pressure difference p is given by $p = \eta\rho g$. With the velocity field $\mathbf{V} = (u, 0, w)$, at the bottom $z = 0$, we have $w = 0$. On the surface $z = h+\eta$, the kinematic boundary condition is $w = \eta_t + u\eta_x$. The continuity and momentum equations and boundary conditions can be expressed as follows:

$$\begin{aligned} &u_x + w_z = 0, \\ &u_t + uu_x + wu_z + \frac{1}{\rho}p_x = 0, \\ &w_t + uw_x + ww_z + \frac{1}{\rho}p_z = 0, \\ &w = \eta_t + u\eta_x \ \text{ on } \ z = h + \eta, \\ &w = 0 \ \text{ on } \ z = 0. \end{aligned} \tag{2.2}$$

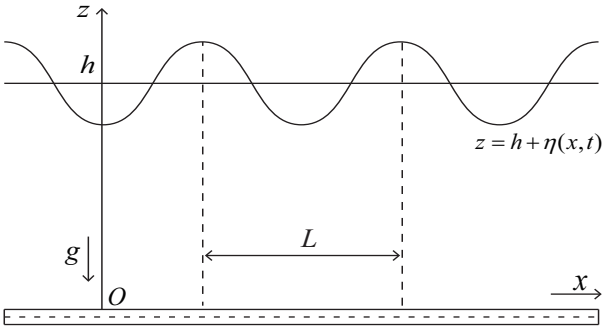

Figure 1. Sketch of the shallow water wave.

We define dimensionless parameters as $\varepsilon = \lambda/h$ and $\delta = h/L$, with λ representing the characteristic

wave amplitude, and use these to express physical quantities in a non-dimensional form:

$$\begin{aligned} &\eta \to a\eta, \quad x \to Lx, \quad z \to zh, \quad t \to \frac{L}{\sqrt{gh}}t, \\ &p \to \varepsilon\rho gh, \quad u \to \sqrt{gh}(\tilde{U}(z) + \varepsilon u), \quad w \to \varepsilon\delta\sqrt{gh}w, \end{aligned} \tag{2.3}$$

where $u = \tilde{U}(z)$ $(0 \le z \le h)$, $w = 0$, $\eta = 0$, and $p = 0$ constitutes an exact solution to Eq (2.2), and the system of dimensionless variables is

$$u_t + \tilde{U}u_x + w\tilde{U}' + \varepsilon(uu_x + wu_z) + p_x = 0, \tag{2.4}$$

$$\delta^2(w_t + \tilde{U}w_x + \varepsilon(uw_x + ww_z)) + p_z = 0, \tag{2.5}$$

$$u_x + w_z = 0, \tag{2.6}$$

$$w = \eta_t + (\tilde{U} + \varepsilon u)\eta_x \ \text{ on } \ z = 1 + \varepsilon\eta, \tag{2.7}$$

$$w = 0 \ \text{ on } \ z = 0. \tag{2.8}$$

We examine a linear shear defined by $\tilde{U}(z) = Az$, where A is a constant and $0 \le z \le 1$. When $A > 0$, the flow is advancing in the positive x-direction with associated vorticity

$$\omega - A = \varepsilon(u_z - \delta^2 w_x). \tag{2.9}$$

We seek a solution where the vorticity is constant, specifically $\omega = A$. Therefore

$$u_z = \delta^2 w_x. \tag{2.10}$$

This assumption essentially involves examining approximate wave solutions that result from interactions between an underlying shear flow and an irrotational disturbance of that flow. With Eqs (2.6), (2.8), and (2.10), it follows that

$$u = u_0 - \frac{1}{6}\varepsilon c u_0^2 - \frac{1}{2}\delta^2 z^2 u_{0,xx} + O(\varepsilon^2, \delta^4, \varepsilon\delta^2), \tag{2.11}$$

$$w = -zu_{0,x} + \frac{1}{3}\varepsilon c u_0 u_{0,x} + \frac{1}{6}\delta^2 z^3 u_{0,xxx} + O(\varepsilon^2, \delta^4, \varepsilon\delta^2), \tag{2.12}$$

where $u_0(x, t)$ represents the leading-order approximation for u. It is important to note that u_0 is independent of z because, as shown in (2.10), u_z approaches zero as $\delta \to 0$.

From (2.7), (2.11), and (2.12), we derive

$$\eta_t + A\eta_x + \left[(1 + \varepsilon\eta)u_0 + \varepsilon\frac{A}{2}\eta^2\right]_x - \frac{1}{3}\varepsilon c u_0 u_{0,x} - \frac{1}{6}\delta^2 u_{0,xxx} = 0, \tag{2.13}$$

where the terms of order $O(\varepsilon^2, \delta^4, \varepsilon\delta^2)$ have been ignored. From the Eqs (2.5), (2.7), (2.11), and (2.12), we have

$$p = \eta - \delta^2\Big(\frac{1-z^2}{2}u_{0,xt} + \frac{1-z^3}{3}Au_{0,xx}\Big). \tag{2.14}$$

Then the Eq (2.4) gives

$$\Big(u_0 - \frac{1}{6}\varepsilon c u_0^2 - \frac{1}{2}\delta^2 u_{0,xx}\Big)_t + \varepsilon u_0 u_{0,x} + \eta_x - \frac{1}{3}\delta^2 A u_{0,xxx} = 0. \tag{2.15}$$

Letting $\varepsilon \to 0$ and $\delta \to 0$, the following system of linear equations is derived from (2.13) and (2.15) as

$$u_{0,t} + \eta_x = 0, \tag{2.16}$$
$$\eta_t + A\eta_x + u_{0,x} = 0, \tag{2.17}$$

which gives

$$\eta_{tt} + A\eta_{tx} - \eta_{xx} = 0, \tag{2.18}$$

whose traveling wave solution of the form $\eta = \eta(x - ct)$, where c is the wave velocity, satisfies

$$c^2 - Ac = 1. \tag{2.19}$$

Making use of Eq (2.19) and introducing

$$r = u_0 - \frac{1}{6}\varepsilon c u_0^2 - \delta^2(\frac{1}{2} - \frac{A}{3c})u_{0,xx} = u_0 - \frac{1}{6}\varepsilon c u_0^2 - \delta^2(\frac{1}{6} + \frac{1}{3c^2})u_{0,xx}. \tag{2.20}$$

Equation (2.15) can be expressed as

$$r_t + \varepsilon r r_x + \eta_x = 0. \tag{2.21}$$

Furthermore, Eq (2.13) with a shift of $\eta \to q - \frac{1}{\varepsilon}$ becomes

$$q_t + \varepsilon(1 + \frac{Ac}{2})(qu_0)_x - \frac{1}{3}\varepsilon c u_0 u_{0,x} - \frac{1}{6}\delta^2 u_{0,xxx} = 0, \tag{2.22}$$

or

$$q_t + \varepsilon\frac{1+c^2}{2}(qW)_x - \frac{1}{3}\varepsilon q_x W - \frac{1}{6}\delta^2 W_{xxx} = 0. \tag{2.23}$$

Letting $c^2 = \frac{1}{3}$ and $\delta^2 = \pm\frac{3}{2}$, and taking the scaling transform in (2.21) and (2.23), lead to the first member of the JM hierarchy:

$$\begin{aligned} &r_t + \frac{3}{2}r r_x + q_x = 0, \\ &q_t + q r_x + \frac{1}{2}q_x r \mp \frac{1}{4}r_{xxx} = 0, \end{aligned} \tag{2.24}$$

which corresponds to the good JM ($\delta^2 = \frac{3}{2}$) and bad JM ($\delta^2 = -\frac{3}{2}$) system. The first member of the JM hierarchy is integrable and has a corresponding Lax pair

$$\psi_x = U\psi, \;\; \psi_t = V\psi, \tag{2.25}$$

with

$$U = \begin{pmatrix} 0 & 1 \\ \sigma\zeta^2 + \zeta r - \sigma q & 0 \end{pmatrix},$$
$$V = \begin{pmatrix} \frac{1}{4}r_x & \sigma\zeta - \frac{r}{2} \\ \zeta^3 + \frac{1}{2}\sigma\zeta^2 r - \frac{1}{2}\zeta r^2 - \zeta q + \frac{1}{4}r_{xx} + \frac{1}{2}\sigma qr & -\frac{1}{4}r_x \end{pmatrix}, \tag{2.26}$$

where ζ is the spectral parameter, and $\sigma = -1$ and $\sigma = 1$ correspond to the Lax pair of the good JM system and bad JM system, respectively.

Taking the space part of the Lax pair (2.25) and formulating the time part, we can obtain the second member of the JM hierarchy. To be specific, if $\sigma = -1$ in Eq (1.2), the high-order good JM equation can be obtained. In the present work, we are focusing on the RW solution, periodic solution, and the initial discontinuity problem of the high-order good JM Eq (1.3).

3. The Lax pair and solutions of the high-order good JM equation

The high-order good Jaulent-Miodek Eq (1.3) has a Lax pair of matrix form as in (2.25), but with

$$U = \begin{pmatrix} 0 & 1 \\ -\zeta^2 + \zeta r + q & 0 \end{pmatrix},$$
$$V = \begin{pmatrix} -\frac{1}{4}\zeta r_x - \frac{1}{4}q_x - \frac{3}{8}rr_x & \zeta^2 + \frac{1}{2}r\zeta + \frac{1}{2}q + \frac{3}{8}r^2 \\ V_{21} & \frac{1}{4}\zeta r_x + \frac{1}{4}q_x + \frac{3}{8}rr_x \end{pmatrix}, \tag{3.1}$$

where $V_{21} = -\zeta^4 + \frac{1}{2}\zeta^3 r + (\frac{1}{2}q + \frac{r^2}{8})\zeta^2 + (-\frac{1}{4}r_{xx} + \frac{3}{8}r^3 + rq)\zeta - \frac{3}{8}rr_{xx} - \frac{1}{4}q_{xx} - \frac{3}{8}r_x^2 + \frac{3}{8}qr^2 + \frac{q^2}{2}$. By compatibility conditions $(\psi_x)_t = (\psi_t)_x$ for any ζ, the good Jaulent-Miodek Eq (1.3) is reproduced. The Lax pair of operator form of (1.3) is

$$\psi_{xx} = \mathcal{A}\psi, \quad \psi_t = -\frac{1}{2}\mathcal{B}_x\psi + \mathcal{B}\psi_x, \tag{3.2}$$

where $\mathcal{A} = -\zeta^2 + \zeta r + q$ and $\mathcal{B} = \zeta^2 + \frac{1}{2}r\zeta + \frac{1}{2}q + \frac{3}{8}r^2$. The spatial linear differential Eq (3.2) is second order, which has two independent solutions $\psi_+(x,t)$ and $\psi_-(x,t)$. Their product, $g = \psi_+\psi_-$, is a squared basis function that satisfies the third-order differential equation

$$g_{xxx} - 2\mathcal{A}_x g - 4\mathcal{A}g_x = 0. \tag{3.3}$$

Equation (3.3) multiplied by g, and integrated with respect with x once gives

$$\frac{1}{2}gg_{xx} - \frac{1}{4}g_x^2 - \mathcal{A}g^2 = P(\zeta), \tag{3.4}$$

where $P(\zeta)$ is the integration constant that depends solely on ζ. The time dependence of $g(x,t)$ is governed by the differential equation

$$g_t = \mathcal{B}g_x - \mathcal{B}_x g, \tag{3.5}$$

which can be expressed as a conservation law

$$\frac{\partial}{\partial t}\Big(\frac{1}{g}\Big) = \frac{\partial}{\partial x}\Big(\frac{\mathcal{B}}{g}\Big). \tag{3.6}$$

Next, we apply the Flaschka-Forest-McLaughlin (FFM) method [35] to study the rarefaction waves and periodic waves of Eq (1.3).

3.1. Rarefaction wave solution

Consider the step-like initial data:

$$r(x,t=0)=\begin{cases} r^L \ \text{ for } \ x<0, \\ r^R \ \text{ for } \ x>0, \end{cases} \qquad q(x,t=0)=\begin{cases} q^L \ \text{ for } \ x<0, \\ q^R \ \text{ for } \ x>0. \end{cases} \tag{3.7}$$

The initial conditions are discontinuous at some point, and it is usually necessary to divide the problem into multiple regions within each region where the initial conditions are continuous. We introduce weak solutions to deal with discontinuities. Commonly used methods to deal with step-like initial value problems include the Riemann-Hilbert (RH) method, Whitham modulation theory method, and numerical calculation method. The RH method [36–38] is suitable for situations where analytical solutions are required, while the Whitham method is more suitable for analyzing the dynamic evolution of strong nonlinear phenomena.

By choosing the simplest constant form of g, we get the rarefaction wave solution of the Eq (1.3). Taking

$$g=1, \ \ P(\zeta)=(\zeta-\zeta_1)(\zeta-\zeta_2)=\zeta^2-s_1\zeta+s_2, \tag{3.8}$$

and substituting (3.8) into Eq (3.4), we obtain

$$r=s_1=\zeta_1+\zeta_2, \ \ q=-s_2=-\zeta_1\zeta_2, \tag{3.9}$$

which can be solved for ζ_1 and ζ_2 as follows:

$$\zeta_1=\frac{1}{2}(r+\sqrt{r^2+4q}), \ \ \zeta_2=\frac{1}{2}(r-\sqrt{r^2+4q}). \tag{3.10}$$

By introducing scaling transform $g\to g/\sqrt{P(\zeta)}$, and from (3.6) and $(3.8)_1$, the conservation law is

$$\frac{\partial}{\partial t}(\sqrt{P(\zeta)})-\frac{\partial}{\partial x}\Big[(\zeta^2+\frac{1}{2}r\zeta+\frac{1}{2}q+\frac{3}{8}r^2)\sqrt{P(\zeta)}\Big]=0. \tag{3.11}$$

Expanding the partial derivative in Eq (3.11), we have

$$\frac{\partial\zeta}{\partial t}-\Big[\zeta^2+\frac{1}{2}(\zeta_1+\zeta_2)\zeta-\frac{1}{2}\zeta_1\zeta_2+\frac{3}{8}(\zeta_1+\zeta_2)^2\Big]\frac{\partial\zeta}{\partial x}=0, \tag{3.12}$$

and taking $\zeta=\zeta_1$ and $\zeta=\zeta_2$, we obtain the zero-phase Whitham modulation equations

$$\begin{aligned} &\frac{\partial\zeta_1}{\partial t}-(\frac{15}{8}\zeta_1^2+\frac{3}{4}\zeta_1\zeta_2+\frac{3}{8}\zeta_2^2)\frac{\partial\zeta_1}{\partial x}=0, \\ &\frac{\partial\zeta_2}{\partial t}-(\frac{15}{8}\zeta_2^2+\frac{3}{4}\zeta_1\zeta_2+\frac{3}{8}\zeta_1^2)\frac{\partial\zeta_2}{\partial x}=0. \end{aligned} \tag{3.13}$$

By introducing similar variable $\xi=x/t$, we have

$$\frac{\partial\zeta_{1,2}}{\partial\xi}(\upsilon_{1,2}-\xi)=0, \ \ \upsilon_{1,2}=-\frac{3}{8}(5\zeta_{1,2}^2+\frac{3}{4}\zeta_1\zeta_2+\zeta_{2,1}^2). \tag{3.14}$$

Corresponding to the initial conditions (3.7), the initial value of $\zeta_{1,2}$ is also discontinuous. For Eq (3.14), there are several forms of the solution:

$$\begin{aligned} &\text{(i)}\begin{cases}\zeta_1 = \text{const},\\ \zeta_2 = \text{const},\end{cases} \quad \text{(ii)}\begin{cases}\zeta_1 = \text{const},\\ \upsilon_2 = \xi,\end{cases} \quad \text{(iii)}\begin{cases}\zeta_2 = \text{const},\\ \upsilon_1 = \xi,\end{cases}\\ &\text{(iv)}\begin{cases}\zeta_1 = \zeta_2 = \zeta,\\ \zeta = \pm\frac{\sqrt{3}}{3}\sqrt{-\xi},\end{cases} \quad \text{(v)}\begin{cases}\zeta_1 = -\zeta_2 = \zeta, \zeta > 0,\\ \zeta = \frac{\sqrt{6}}{3}\sqrt{-\xi}.\end{cases}\end{aligned} \tag{3.15}$$

For case (i), the solutions for r and q are constants, and we refer to this as the plateau (PL). Obviously, the system of Eqs (3.14) has constant solutions. Other solutions are rarefaction waves (RWs), which are stable, localized waves whose shape remains unchanged during propagation and are able to propagate without energy loss. Choosing some special initial values, the structures of the corresponding solutions r and q for cases (ii)–(iv) are shown in the middle region of Figure 2 with MATLAB software. In the general case, this type of wave can connect uniform flows with equal values of the corresponding Riemann invariants. For case (v), from (3.9), the solution for r is 0. As a special solution, RWs can occur in many physical systems, such as Bose-Einstein condensates, superfluids, water waves, light waves, and plasmas. Understanding these fluctuations helps to further the study of phase transitions and critical phenomena.

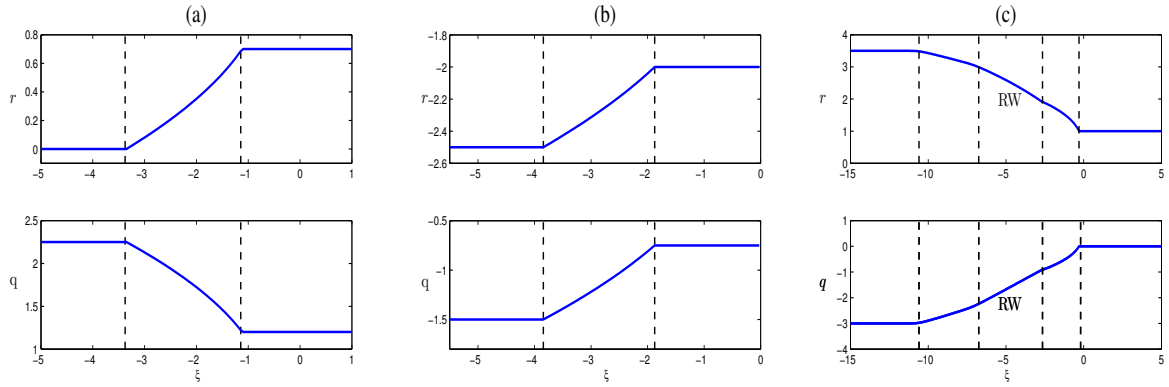

Figure 2. The profiles of RW solutions. The parameters are (a) $\zeta_1^L = \zeta_1^R = 1.5, \zeta_2^L = -1.5, \zeta_2^R = -0.8$; (b) $\zeta_1^L = -1, \zeta_1^R = -0.5, \zeta_2^L = \zeta_2^R = 1.5$; (c) $\zeta_1^L = 2, \zeta_1^R = 1, \zeta_2^L = 1.5, \zeta_2^R = 0$.

3.2. Periodic wave solution

Now, we are interested in the one-phase periodic solutions of Eq (1.3). They are distinguished by the condition that $P(\zeta)$ in (3.4) is a fourth-degree polynomial of the form:

$$P(\zeta) = \prod_{i=1}^{4}(\zeta - \zeta_i) = \zeta^4 - s_1\zeta^3 + s_2\zeta^2 - s_3\zeta + s_4, \tag{3.16}$$

where

$$\begin{aligned} s_1 &= \zeta_1 + \zeta_2 + \zeta_3 + \zeta_4, \\ s_2 &= \zeta_1\zeta_2 + \zeta_1\zeta_3 + \zeta_1\zeta_4 + \zeta_2\zeta_3 + \zeta_2\zeta_4 + \zeta_3\zeta_4, \\ s_3 &= \zeta_1\zeta_2\zeta_3 + \zeta_1\zeta_2\zeta_4 + \zeta_1\zeta_3\zeta_4 + \zeta_2\zeta_3\zeta_4, \\ s_4 &= \zeta_1\zeta_2\zeta_3\zeta_4. \end{aligned} \tag{3.17}$$

Let the polynomial $P(\zeta)$ have zeros ζ_i (for $i = 1, 2, 3, 4$). For definiteness, we choose to order the zeros ζ_i according to

$$\zeta_1 \geq \zeta_2 \geq \zeta_3 \geq \zeta_4. \tag{3.18}$$

We find that $g(x, t)$ is a first-degree polynomial in ζ of the form:

$$g(x, t) = \phi(\zeta - \mu(x, t)), \tag{3.19}$$

where $\phi = 1$, and μ is related to $q(x, t)$ and $r(x, t)$ through the following relations:

$$\begin{aligned} r(x, t) &= s_1 - 2\mu(x, t), \\ q(x, t) &= 2s_1\mu(x, t) - s_2 - 3\mu^2(x, t), \end{aligned} \tag{3.20}$$

which result from comparing the coefficients of different powers of ζ on both sides of Eq (3.4). With $\zeta = \mu$ substituted into Eq (3.4), we obtain

$$\mu_x = 2\sqrt{-P(\mu)}, \tag{3.21}$$

while a similar substitution into Eq (3.5) gives

$$\mu_t = (\mu^2 + \frac{3}{8}r^2 + \frac{1}{2}r\mu + \frac{1}{2}q)\mu_x = -\frac{1}{2}(s_2 - \frac{3}{4}s_1^2)\mu_x. \tag{3.22}$$

Equations (3.21) and (3.22) are the Dubrovin form in the one-phase case. Hence, $\mu(x, t)$, $q(x, t)$, and $r(x, t)$ depend on

$$\theta = x - Vt, \tag{3.23}$$

where

$$V = -\frac{3}{8}(\zeta_1^2 + \zeta_2^2 + \zeta_3^2 + \zeta_4^2) - \frac{1}{4}\zeta_1(\zeta_2 + \zeta_3 + \zeta_4) - \frac{1}{4}\zeta_2(\zeta_3 + \zeta_4) - \frac{1}{4}\zeta_3\zeta_4 \tag{3.24}$$

is the phase velocity.

The function μ satisfies the equation

$$\mu_\theta = 2\sqrt{-P(\mu)}. \tag{3.25}$$

It can be inferred from Eq (3.19) that the μ must be real. For the fourth-degree polynomial in (3.16), the real solution of Eq (3.25) corresponds to μ oscillating within one of the two possible intervals,

$$\zeta_4 \leq \mu \leq \zeta_3 \ \text{ or } \ \zeta_2 \leq \mu \leq \zeta_1, \tag{3.26}$$

within which $P(\mu)$ is positive. It is well established that the solution to Eq (3.25), given the initial condition in (3.26), can be expressed using elliptic functions.

For the case

$$\zeta_4 \leq \mu \leq \zeta_3, \tag{3.27}$$

the periodic wave solution (Figure 3) of Eq (3.25) with the initial condition $\mu(0) = \zeta_4$ is given by

$$\mu(\theta) = \zeta_3 - \frac{(\zeta_3 - \zeta_4)\mathrm{cn}^2(W, m)}{1 + \frac{\zeta_3 - \zeta_4}{\zeta_1 - \zeta_3}\mathrm{sn}^2(W, m)}, \tag{3.28}$$

where

$$\Delta_{sj} = \zeta_s - \zeta_j, \quad W = \sqrt{\Delta_{13}\Delta_{24}}\theta, \quad m = \frac{\Delta_{12}\Delta_{34}}{\Delta_{13}\Delta_{24}} \tag{3.29}$$

is the modulus of the Jacobi elliptic functions sn and cn. The wavelength is given by

$$L = \oint \frac{\mathrm{d}\mu}{\sqrt{-P(\mu)}} = 2\int_{\zeta_4}^{\zeta_3} \frac{\mathrm{d}\mu}{\sqrt{-P(\mu)}} = \frac{2K(m)}{\sqrt{\Delta_{31}\Delta_{42}}}, \tag{3.30}$$

where $K(m)$ is the complete elliptic integral of the first kind. Substituting (3.28) into (3.20), one can obtain the one-phase periodic wave solutions $r(x, t)$ and $q(x, t)$ to Eq (1.3). A periodic wave is a wave phenomenon that occurs repeatedly in a certain time and space.

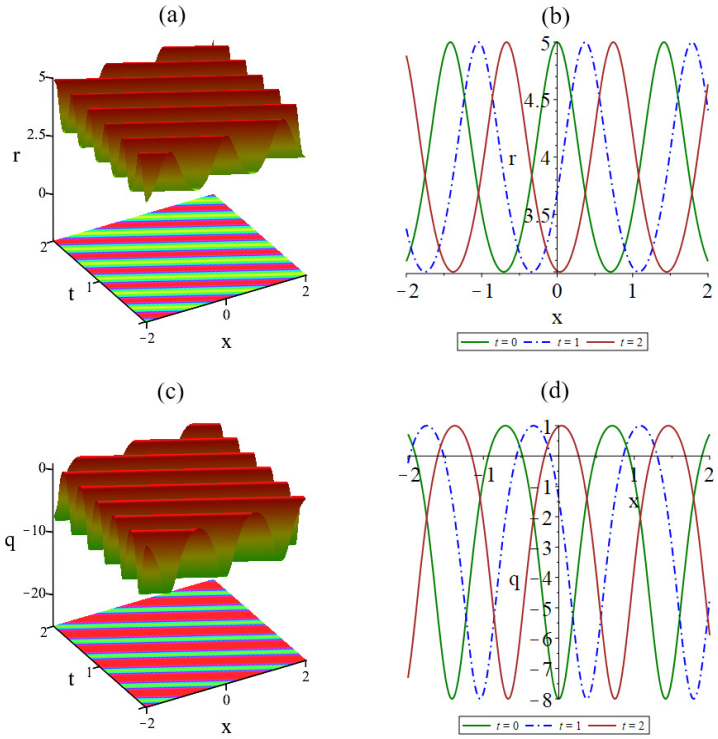

Figure 3. The periodic wave solution (3.28) with parameters $\zeta_1 = 3, \zeta_2 = 1, \zeta_3 = 0$, and $\zeta_4 = -1$. (a) and (b) are the r profiles, and (c) and (d) are the q profiles.

In the soliton limit $\zeta_2 \to \zeta_3$, we form $(3.29)_3$ and then $\Delta_{12} \to \Delta_{13}$ and $\Delta_{24} \to \Delta_{34}$ yield $m \to 1$. Then, the wavelength tends to infinity and the solution (3.28) reduced to a soliton

$$\mu(\theta) = \zeta_3 - \frac{\Delta_{34}}{\cosh^2(\varpi) + \frac{\Delta_{34}}{\Delta_{13}} \sinh^2(\varpi)}, \quad \varpi = \sqrt{\Delta_{13}\Delta_{34}}\theta. \tag{3.31}$$

Figure 4(a),(b) shows the soliton solution (3.31) with the help of Maple software, where (a) is a bell-type soliton, and (b) is an anti-bell-type soliton. The small amplitude limit $m \to 0$ can be reached in two ways: $\zeta_3 \to \zeta_4$ and $\zeta_2 \to \zeta_1$. If $\zeta_3 \to \zeta_4$, the periodic wave solution (3.28) reduces to constant ζ_4. If $\zeta_2 \to \zeta_1$, we obtain

$$\mu(\theta) = \zeta_3 - \frac{\Delta_{34}\cos^2(\omega)}{1 + \frac{\Delta_{34}}{\Delta_{13}} \sin^2(\omega)}, \quad \omega = \sqrt{\Delta_{13}\Delta_{14}}\theta, \tag{3.32}$$

which is a trigonometric solution (see Figure 4(c),(d)). $\zeta_3 \to \zeta_1$, we obtain the algebraic soliton solution:

$$\mu(\theta) = \zeta_1 - \frac{\Delta_{14}}{1 + (\Delta_{14})^2\theta^2}. \tag{3.33}$$

Figure 5 is the plot of an algebraic soliton.

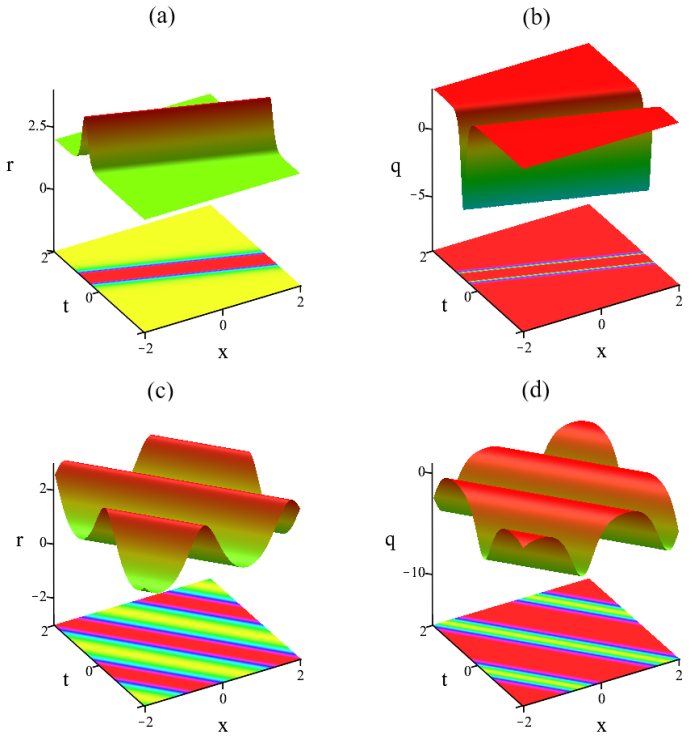

Figure 4. (a) and (b) are the soliton solution (3.31) with parameters $\zeta_1 = 3, \zeta_2 = \zeta_3 = 0$, and $\zeta_4 = -1$ and (c) and (d) are the trigonometric solutions (3.32) with parameters $\zeta_1 = \zeta_2 = 1, \zeta_3 = 0$, and $\zeta_4 = -1$.

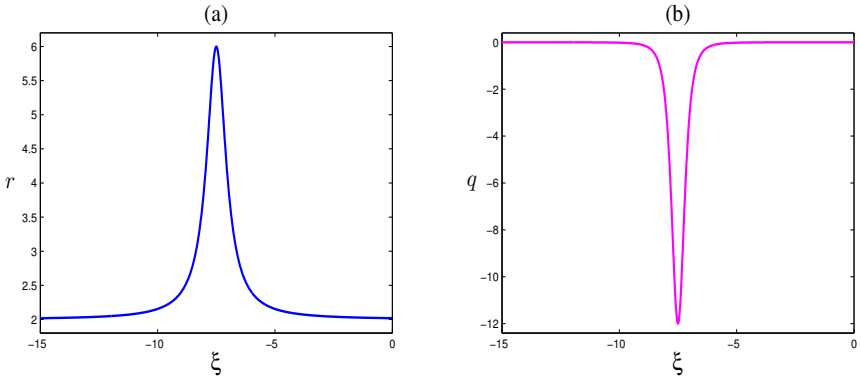

Figure 5. An algebraic soliton solution ($\zeta_1 = 2, \zeta_4 = 0$). (a) is the r profile, and (b) is the q profile.

In a similar way, for the case

$$\zeta_2 \leq \mu \leq \zeta_1, \tag{3.34}$$

the periodic wave solution (Figure 6) is of the form ($\mu(0) = \zeta_1$)

$$\mu(\theta) = \zeta_2 + \frac{\Delta_{12}\mathrm{cn}^2(W,m)}{1 + \frac{\Delta_{12}}{\Delta_{24}}\mathrm{sn}^2(W,m)}, \tag{3.35}$$

with the same definitions for W and m as in (3.29), where the wavelength is given by

$$L = \oint \frac{\mathrm{d}\mu}{\sqrt{-P(\mu)}} = 2\int_{\zeta_2}^{\zeta_1} \frac{\mathrm{d}\mu}{\sqrt{-P(\mu)}} = \frac{2K(m)}{\sqrt{\Delta_{13}\Delta_{24}}}, \tag{3.36}$$

which equals the wavelength in the interval $[\zeta_4, \zeta_3]$. So, in the following, the wavelength is uniformly represented by $\oint \frac{\mathrm{d}\mu}{\sqrt{-P(\mu)}}$. Substituting (3.35) into (3.20), the periodic wave solution $r(x,t)$ and $q(x,t)$ to Eq (1.3) in interval $[\zeta_2, \zeta_1]$ can be obtained. In the limit $\zeta_3 \to \zeta_4 (m \to 0)$, we have

$$\mu(\theta) = \zeta_2 + \frac{\Delta_{12}\cos^2(\omega)}{1 + \frac{\zeta_1-\zeta_2}{\zeta_2-\zeta_4}\sin^2(\omega)}, \quad \omega = \sqrt{\Delta_{14}\Delta_{24}}\theta, \tag{3.37}$$

which is another trigonometric solution (see Figure 7(a),(b)), and the profile of q has a bimodal structure (see Figure 8). In the soliton limit $\zeta_2 \to \zeta_3$, the periodic wave solution (3.35) reduces to

$$\mu(\theta) = \zeta_3 + \frac{\Delta_{13}}{\cosh^2(\varpi) + \frac{\Delta_{13}}{\Delta_{34}}\sinh^2(\varpi)}. \tag{3.38}$$

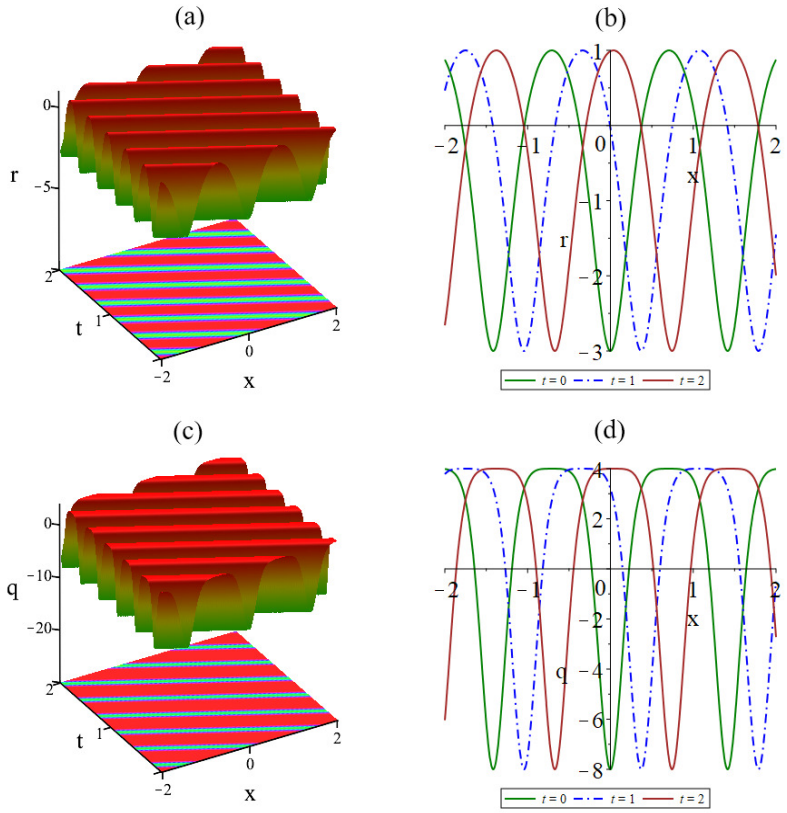

Figure 6. The periodic wave solution (3.35) with parameters $\zeta_1 = 3, \zeta_2 = 1, \zeta_3 = 0$, and $\zeta_4 = -1$. (a) and (b) are the r profiles, and (c) and (d) are the q profiles.

$\zeta_2 \to \zeta_4$, we obtain the algebraic soliton solution (3.33) (see Figure 7(c),(d)). For another small amplitude limit $\zeta_1 \to \zeta_2$, the periodic wave solution (3.35) reduces to the constant solution ζ_2.

For conservation law (3.6), introducing the scaling transform $g/\sqrt{P(\zeta)}$, and averaging the space variable x over one wavelength L, we obtain the one-phase Whitham-JM modulation equations as follows:

$$\frac{\partial \zeta_i}{\partial t} + \upsilon_i \frac{\partial \zeta_i}{\partial x} = 0, \quad i = 1, 2, 3, 4, \tag{3.39}$$

where the Whitham velocities υ_i can be written as

$$\upsilon_i(\zeta_1, \zeta_2, \zeta_3, \zeta_4) = (1 - \frac{L}{\partial_{\zeta_i} L} \partial_{\zeta_i}) V, \tag{3.40}$$

and ζ_i $(i = 1, \ldots, 4)$ are Riemann invariants. For initial data (3.7), the initial data of Riemann invariants are

$$\zeta_-(x, 0) = \begin{cases} \zeta_-^L \text{ for } x < 0, \\ \zeta_-^R \text{ for } x > 0, \end{cases} \qquad \zeta_+(x, 0) = \begin{cases} \zeta_+^L \text{ for } x < 0, \\ \zeta_+^R \text{ for } x > 0. \end{cases} \tag{3.41}$$

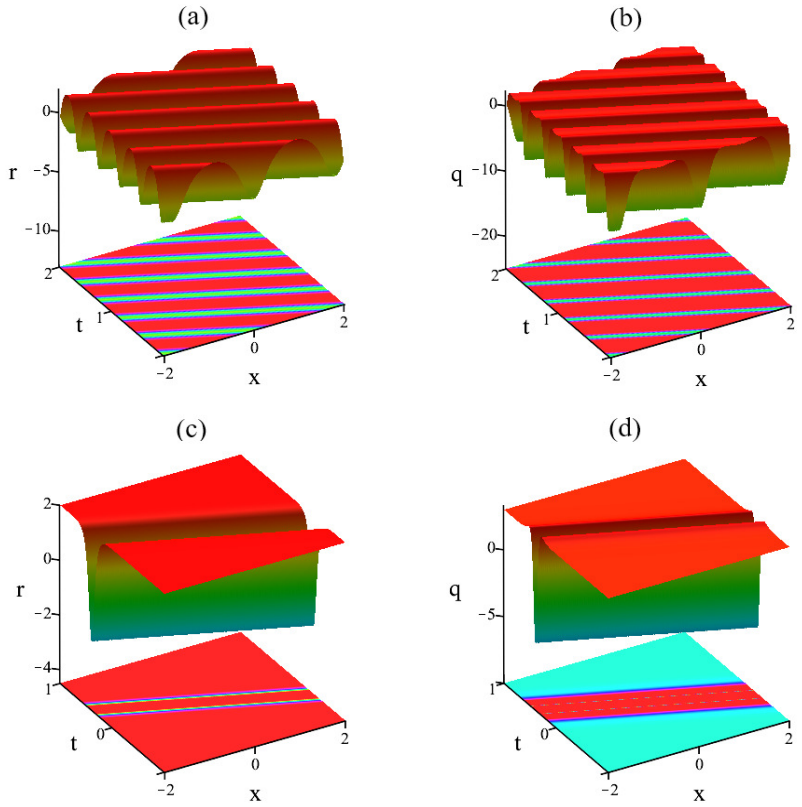

Figure 7. (a) and (b) are the trigonometric solution (3.37) with parameters $\zeta_1 = 3, \zeta_2 = 1$, and $\zeta_3 = \zeta_4 = 0$, (c) and (d) are the soliton solutions (3.38) with parameters $\zeta_1 = 3, \zeta_2 = \zeta_3 = 1$, and $\zeta_4 = -1$.

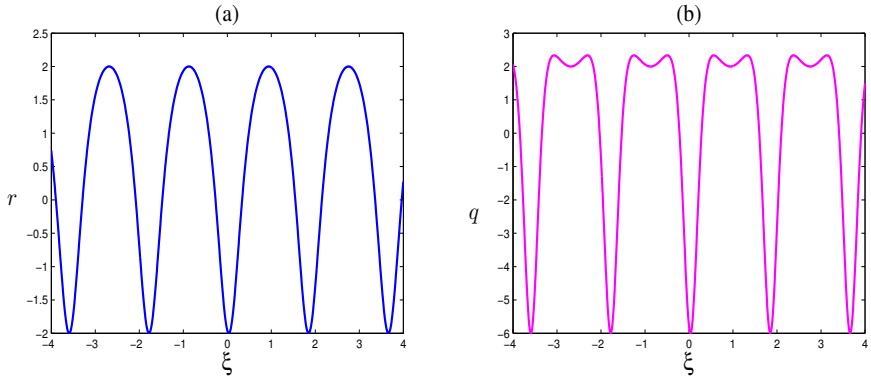

Figure 8. A trigonometric solution ($\zeta_1 = 3, \zeta_2 = 1, \zeta_3 = \zeta_4 = 0$). (a) is the r profile, and (b) is the q profile.

Without loss of generality, we choose $\zeta_+^L = 3.5, \zeta_-^L = 0, \zeta_+^R = 2.5, \zeta_-^R = 2$, and the distribution of the Riemman invariants ζ_i are shown in Figure 9(a) at $t = 1$. The wave profiles of solutions r and q are Figure 9(b),(c). When waves move fast enough into a riverbed or narrow channel, a similar wave structure forms near a tidal front. From left to right, the first, third, and fifth regions are plateaus, the

second region is a rarefaction wave, and the fourth region is a dispersion shock wave, i.e., a periodic wave region. The left and right boundary points of the middle three regions have continuity. The left and right boundary velocities of RW are

$$\upsilon_{RW}^{L} = -\frac{3}{8}[5(\zeta_{+}^{L})^2 + \frac{4}{3}\zeta_{+}^{L}\zeta_{-}^{L} + (\zeta_{-}^{L})^2], \quad \upsilon_{RW}^{R} = -\frac{3}{8}[5(\zeta_{+}^{R})^2 + \frac{4}{3}\zeta_{+}^{R}\zeta_{-}^{L} + (\zeta_{-}^{L})^2]. \tag{3.42}$$

The left and right boundary velocities of DSW are

$$\begin{aligned} \upsilon_{DSW}^{L} &= -\Big\{\frac{3}{8}(\zeta_{+}^{R})^2 + \frac{1}{2}\zeta_{+}^{R}\zeta_{-}^{R} + \frac{1}{4}\zeta_{+}^{R}\zeta_{-}^{L} + \frac{3}{8}(\zeta_{-}^{L})^2 + \frac{1}{2}\zeta_{-}^{R}\zeta_{-}^{L} + (\zeta_{-}^{R})^2\Big\}, \\ \upsilon_{DSW}^{R} &= -3(\zeta_{-}^{L})^2 - \frac{3}{8}\frac{(\zeta_{+}^{R} - \zeta_{-}^{R})^2(\zeta_{+}^{R} + \zeta_{-}^{R} + 2\zeta_{-}^{L})}{\zeta_{+}^{R} + \zeta_{-}^{R} - 2\zeta_{-}^{L}}. \end{aligned} \tag{3.43}$$

It is worth noting that $\zeta_{+}^{L} > \zeta_{-}^{L}$ and $\zeta_{+}^{R} > \zeta_{-}^{R}$, and the initial value data of different-size relations correspond to different wave structures of Eq (1.3).

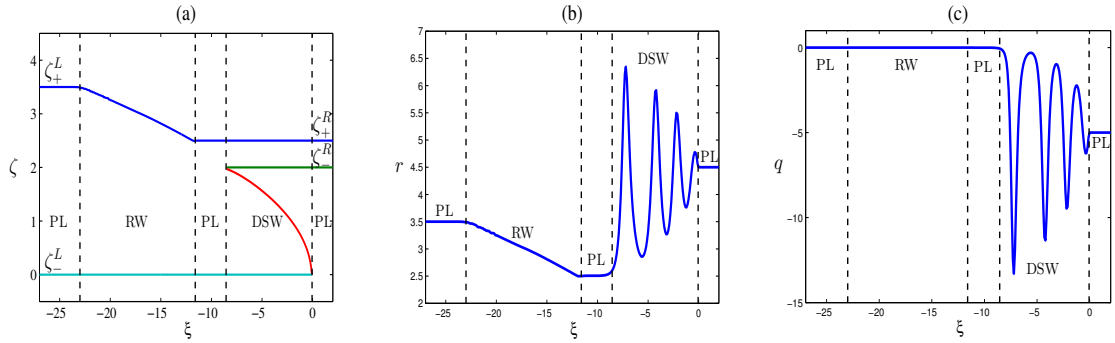

Figure 9. (a) shows the profiles of Riemann invariants, and (b) and (c) are the profiles of r and q for step-like initial data $\zeta_{+}^{L} = 3.5, \zeta_{-}^{L} = 0, \zeta_{+}^{R} = 2.5$, and $\zeta_{-}^{R} = 2$.

4. Conclusions

In conclusion, this study explores the physical significance of the Jaulent-Miodek model based on Euler's equation, presenting both rarefaction wave and periodic solutions using the traveling wave technique and similar transforms. The findings illustrate that the Jaulent-Miodek model effectively describes shallow water wave motion (see Figure 1), and Eq (1.3) exhibits Lax integrability. By introducing zero-phase and one-phase squared basis functions g, the Whitham-JM equations (Eqs (3.13) and (3.39)) are derived. Analyzing step-like initial data reveals the structural profiles of RW and DSW solutions through Riemann invariants. The dynamic behaviors are visually depicted in Figures 2 and 9. Additionally, cn wave solutions (3.28) and (3.35), including periodic waves, solitons, trigonometric solutions, and algebraic soliton solutions (Figures 3–8), are explored. These results contribute significantly to understanding discontinuous initial value problems through Whitham modulation theory (Figure 9). It is worth noting that the periodic wave of the equation is obtained by the FFM method, which is suitable for the model of a quasi-linear hyperbolic system after ignoring the dispersion term, such as the KdV equation, NLS equation, Kaup-Boussinesq equation, etc. In summary, this research underscores the importance of periodic wave solutions and provides a foundational basis for future studies in addressing discontinuous initial value problems.

There are many types of discontinuous initial values, and this paper mainly focuses on step-like initial values. The research group will later study the initial values for the infinite square well and finite square barrier. The infinite square well and finite square barrier are fundamental models for understanding and applying quantum mechanics. They hold significant importance in theoretical research, experimental design, and practical engineering applications. In addition, fractional-order differential equations have rich physical applications [39–41]. The dynamical behavior of fractional-order differential equations is studied by analytical and numerical methods for further exploration and application in various ways scientific and engineering disciplines with great significance.

Author contributions

Wenzhen Xiong: Writing the original draft, data curation, conducting investigations; Yaqing Liu: supervision, ensuring validity of findings. All authors have read and approved the final version of the manuscript for publication.

Acknowledgments

This work is supported by the Beijing Natural Science Foundation (No. 1222005).

Conflict of interest

The authors disclose that there are no identifiable competing financial interests or personal relationships that could potentially influence the findings presented in this research.

References

1. S. Kumar, H. Almusawa, I. Hamild, M. A. Abdou, Abundant closed-form solutions and solitonic structures to an integrable fifth-order generalized nonlinear evolution equation in plasma physics, *Results Phys.*, **26** (2021), 104453. https://doi.org/10.1016/j.rinp.2021.104453
2. X. Y. Gao, In plasma physics and fluid dynamics: Symbolic computation on a (2+1)-dimensional variable-coefficient Sawada-Kotera system, *Appl. Math. Lett.*, **159** (2025), 109262. https://doi.org/10.1016/j.aml.2024.109262
3. G. X. Zhang, P. Huang, B. F. Feng, C. F. Wu, Rogue waves and their patterns in the vector nonlinear Schrödinger equation, *J. Nonlinear Sci.*, **33** (2023), 116. https://doi.org/10.1007/s00332-023-09971-5
4. B. F. Feng, C. Y. Shi, G. X. Wu, C. F. Wu, Higher-order rogue wave solutions of the Sasa-Satsuma equation, *J. Phys. A*, **55** (2022), 235701. https://doi.org/10.1088/1751-8121/ac6917
5. M. A. Helal, Soliton solution of some nonlinear partial differential equations and its applications in fluid mechanics, *Chaos Soliton. Fract.*, **13** (2002), 1917–1929. https://doi.org/10.1016/S0960-0779(01)00189-8
6. X. Y. Gao, Auto-Bäcklund transformation with the solitons and similarity reductions for a generalized nonlinear shallow water wave equation, *Qual. Theor. Dyn. Syst.*, **23** (2024), 181. https://doi.org/10.1007/s12346-024-01034-8

7. X. Y. Gao, Oceanic shallow-water investigations on a generalized Whitham-Broer-Kaup-Boussinesq-Kupershmidt system, *Phys. Fluids*, **35** (2023), 127106. https://doi.org/10.1063/5.0170506
8. L. C. Zhao, C. Liu, Z. Y. Yang, The rogue waves with quintic nonlinearity and nonlineardispersion effects in nonlinear optical fibers, *Commun. Nonlinear Sci.*, **20** (2015), 9–14. https://doi.org/10.1016/j.cnsns.2014.04.002
9. M. Tlidi, K. Panajotov, Two-dimensional dissipative rogue waves due to time-delayed feedback in cavity nonlinear optics, *Chaos*, **27** (2017), 013119. https://doi.org/10.1063/1.4974852
10. X. Y. Gao, Symbolic computation on a (2+1)-dimensional generalized nonlinear evolution system in fluid dynamics, plasma physics, nonlinear optics and quantum mechanics, *Qual. Theor. Dyn. Syst.*, **23** (2024), 202. https://doi.org/10.1007/s12346-024-01045-5
11. Y. Shen, B. Tian, T. Y. Zhou, C. D. Cheng, Multi-pole solitons in an inhomogeneous multi-component nonlinear optical medium, *Chaos Soliton. Fract.*, **171** (2023), 113497. https://doi.org/10.1016/j.chaos.2023.113497
12. S. Burger, K. Bongs, S. Dettmer, W. Ertmer, K. Sengstock, Dark solitons in Bose-Einstein codensates, *Phys. Rev. Lett.*, **83** (1999), 5198–5201. https://doi.org/10.1103/PhysRevLett.83.5198
13. V. E. Zakharov, S. V. Nazarenko, Dynamics of the Bose-Einstein condensation, *Physica D*, **201** (2005), 203–211. https://doi.org/10.1016/j.physd.2004.11.017
14. M. Jaulent, I. Miodek, Nonlinear evolution equations associated with energy-dependent schrödinger potentials, *Lett. Math. Phys.*, **1** (1976), 243–250. https://doi.org/10.1007/BF00417611
15. G. A. El, R. H. J. Grimshaw, M. V. Pavlov, Integrable shallow-water equations and undular bores, *Stud. Appl. Math.*, **106** (2001), 157–186. https://doi.org/10.1111/1467-9590.00163
16. G. B. Whitham, *Linear and nonlinear waves*, New York: John Wiley and Sons, 1974.
17. A. M. Kamchatnov, Whitham equation in the AKNS scheme, *Phys. Lett. A*, **186** (1994), 387–390. https://doi.org/10.1016/0375-9601(94)90699-8
18. G. A. El, V. V. Geogjaev, A. V. Gurevich, A. L. Krylov, Decay of an initial discontinuity in the defocusing NLS hydrodynamics, *Physica D*, **87** (1995), 186–192. https://doi.org/10.1016/0167-2789(95)00147-V
19. Y. J. Kodama, V. U. Pierce, F. R. Tian, On the Whitham equations for the defocusing complex modified KdV equation, *SIAM J. Math. Anal.*, **40** (2008), 1750–1782. https://doi.org/10.1137/070705131
20. S. K. Ivanov, Riemann problem for the light pulses in optical fibers for the generalized Chen-Lee-Liu equation, *Phys. Rev. A*, **101** (2020), 053827. https://doi.org/10.1103/PhysRevA.101.053827
21. T. J. Bridges, D. J. Ratliff, Nonlinear theory for coalescing characteristics in multiphase Whitham modulation theory, *J. Nonlinear Sci.*, **31** (2021), 7. https://doi.org/10.1007/s00332-020-09669-y
22. Y. Q. Liu, D. S. Wang, Exotic wave patterns in Riemann problem of the high-order Jaulent-Miodek equation: Whitham modulation theory, *Stud. Appl. Math.*, **149** (2022), 588–630. https://doi.org/10.1111/sapm.12513

23. A. Abeya, G. Biondini, M. A Hoefer, Whitham modulation theory for the defocusing nonlinear Schrödinger equation in two and three spatial dimensions, *J. Phys. A*, **56** (2023), 025701. https://doi.org/10.1088/1751-8121/acb117
24. Y. Q. Liu, S. J. Zeng, Discontinuous initial value and Whitham modulation for the generalized Gerdjikov-Ivanov equation, *Wave Motion*, **127** (2024), 103276. https://doi.org/10.1016/j.wavemoti.2024.103276
25. J. B. Chen, Quasi-periodic solutions of the negative-order Jaulent-Miodek hierarchy, *Rev. Math. Phys.*, **32** (2020), 2050007. https://doi.org/10.1142/S0129055X20500075
26. Y. Matsuno, Reduction of dispersionless coupled Korteweg-de Vries equations to the Euler-Darboux equation, *J. Math. Phys.*, **42** (2001), 1744–1760. https://doi.org/10.1063/1.1345500
27. R. G. Zhou, The finite-band solution of the Jaulent-Miodek equation, *J. Math. Phys.*, **38** (1997), 2535–2546. https://doi.org/10.1063/1.531993
28. E. G. Fan, Uniformly constructing a series of explicit exact solutions to nonlinear equations in mathematical physics, *Chaos Soliton. Fract.*, **13** (2003), 819–839. https://doi.org/10.1016/S0960-0779(02)00472-1
29. A. M. Wazwaz, The tanh-coth and the sech methods for exact solutions of the Jaulent-Miodek equation, *Phys. Lett. A*, **366** (2007), 85–90. https://doi.org/10.1016/j.physleta.2007.02.011
30. M. S. Iqbal, A. R. Seadawy, M. Z. Baber, M. Qasim, Application of modified exponential rational method to Jaulent-Miodek system leading to exact classical solutions, *Chaos Soliton. Fract.*, **164** (2022), 112600. https://doi.org/10.1016/j.chaos.2022.112600
31. H. Wang, T. C. Xia, Super Jaulent-Miodek hierarchy and its super Hamiltonian structure, conservation laws and its self-consistent sources, *Front. Math. China*, **9** (2014), 1367–1379. https://doi.org/10.1007/s11464-014-0419-x
32. S. Alshammari, M. M. Al-Sawalha, R. Shah, Approximate analytical methods for a fractional-order nonlinear system of Jaulent-Miodek equation with energy-dependent Schrödinger potential, *Fractal Fract.*, **7** (2023), 140. https://doi.org/10.3390/fractalfract7020140
33. R. Ivanov, Two-component integrable systems modelling shallow water waves: The constant vorticity case, *Wave Motion*, **46** (2009), 389–396. https://doi.org/10.1016/j.wavemoti.2009.06.012
34. D. Duthkh, Effects of vorticity on the travelling waves of some shallow water two-component systems, *Discrete Contin. Dyn. Syst.*, **39** (2019), 5521–5541. https://doi.org/10.3934/dcds.2019225
35. H. Flaschka, M. G. Forest, D. W. McLaughlin, Multiphase averaging and the inverse spectral solution of the Korteweg-de Vries equation, *Pure Appl. Math.*, **33** (1980), 739–784. https://doi.org/10.1002/cpa.3160330605
36. A. B. Monnel, I. Egorova, The Toda lattice with step-like initial data. Soliton asymptotics, *Inverse Probl.*, **16** (2000), 955–977. https://doi.org/10.1088/0266-5611/16/4/306
37. Z. Y. Wang, K. Xu, E. G. Fan, The complex MKDV equation with step-like initial data: Large time asymptotic analysis, *J. Math. Phys.*, **64** (2023), 103504. https://doi.org/10.1063/5.0131306
38. L. Lei, S. F. Tian, Y. Q. Wu, Multi-soliton solutions for the nonlocal Kundu-nonlinear Schrödinger equation with step-like initial data, *J. Nonlinear Math. Phys.*, **30** (2023), 1661–1679. https://doi.org/10.1007/s44198-023-00149-x

39. A. S. Alshehry, H. Yasmin, R. Shah, A. Ali, I. Khan, Fractional-order view analysis of Fisher's and foam drainage equations within Aboodh transform, *Eng. Computation.*, **41** (2024), 489–515. https://doi.org/10.1108/EC-08-2023-0475

40. H. Yasmin, A. S. Alshehry, A. H. Ganie, A. M. Mahnashi, Perturbed Gerdjikov-Ivanov equation: Soliton solutions via Bäcklund transformation, *Optik*, **298** (2024), 171576. https://doi.org/10.1016/j.ijleo.2023.171576

41. A. S. Alshehry, H. Yasmin, M. A. Shah, R. Shah, Analyzing fuzzy fractional Degasperis-Procesi and Camassa-Holm equations with the Atangana-Baleanu operator, *Open Phys.*, **22** (2024), 20230191. https://doi.org/10.1515/phys-2023-0191

AIMS Press

© 2024 the Author(s), licensee AIMS Press. This is an open access article distributed under the terms of the Creative Commons Attribution License (https://creativecommons.org/licenses/by/4.0)